Solid State Communications 149 (2009) 1072–1079

Contents lists available at ScienceDirect

Solid State Communications

journal homepage: www.elsevier.com/locate/ssc

Theory of charged impurity scattering in two-dimensional graphene

S. Adam, E.H. Hwang, E. Rossi, S. Das Sarma *

Condensed Matter Theory Center, Department of Physics, University of Maryland, College Park, MD 20742-4111, United States

ARTICLE INFO

Article history:
Received 10 December 2008
Accepted 25 February 2009 by the Guest Editors
Available online 19 March 2009

PACS:
81.05.Uw
73.63.-b
72.10.-d

Keywords:
A. Graphene
D. Electronic transport

ABSTRACT

We review the physics of charged impurities in the vicinity of graphene. The long-range nature of Coulomb impurities affects both the nature of the ground state density profile and graphene's transport properties. We discuss the screening of a single Coulomb impurity and the ensemble averaged density profile of graphene in the presence of many randomly distributed impurities. Finally, we discuss graphene's transport properties due to scattering off charged impurities both at low and high carrier density.

1. Introduction

Graphene is a two-dimensional (2D) sheet of carbon whose atoms arrange in a honeycomb lattice with nearest neighbor atoms forming strong sp_2 bonds. The electronic properties of this material are mostly determined by the p_z orbitals with each carbon atom contributing one electron to a Bloch band whose low-energy properties are adequately described by a Dirac–Weyl effective Hamiltonian. While the study of Dirac Fermions has emerged in several contexts in theoretical condensed matter physics, its experimental realization about three years ago, in the form of gated graphene devices [1–3], where the carrier density can be tuned continuously from electron-like carriers for positive bias to hole-like carriers for negative gate voltage, has prompted a prolific theoretical and experimental effort to understand the properties of this novel material.

Most of the excitement surrounding graphene stems from one of the following peculiar properties: (i) electrons and holes in graphene have a gapless linear dispersion relation in contrast to the parabolic dispersion of other more conventional electron gases; (ii) the carriers in graphene are chiral — a property that has striking consequences such as the "half-integer" quantum Hall Effect [2,3]; and (iii) carriers in graphene live at an exposed almost perfect 2D surface that is amenable to surface probes [4–8] and surface manipulation [9,10]. In addition, we note that there is the potential of mass producing graphene through epitaxial growth methods [11], and that graphene has remarkable mechanical properties [12,13] which only further enhance the interest.

In this perspective, we look at one important aspect of graphene which is the influence of disorder on its ground state and transport properties. We demonstrate that for graphene, charged (i.e. Coulomb) impurities behave qualitatively different from neutral impurities [14–16] and dominate graphene's transport properties at low carrier density. The importance of the Coulomb nature of graphene impurities was highlighted by Ando [17], where by calculating the intraband contribution to the polarizability and absorbing the interband (i.e. electron–hole) contribution into a redefinition of the dielectric constant [18] he showed that charged impurities could explain the conductivity being linear in density, as was seen in experiments [1,19]. Similar conclusions were obtained by Nomura and MacDonald [20] using a "complete screening" model (i.e. $r_s \rightarrow \infty$, see definition below), Cheianov and Fal'ko using a numerical Thomas–Fermi approximation [21] and in Ref. [22] using the full Random Phase Approximation (RPA). Analytic expressions for the RPA polarizability function calculated first in Ref. [23] and then in Refs. [24–26] revealed that for momentum transferred on the Fermi circle (i.e. $q = |\mathbf{k} - \mathbf{k}'| = 2k_F \sin\theta/2 \leq 2k_F$) the graphene dielectric function calculated using the RPA was identical to the much simpler Thomas–Fermi approximation at $T = 0$ (see Fig. 1). This then made it possible to calculate the RPA Boltzmann conductivity analytically [27], and the dependence of graphene's conductivity on the fine-structure constant $r_s \equiv e^2/(\hbar v_F \kappa)$ was recently verified experimentally [10]. The importance of Coulomb scattering in explaining the observed graphene transport properties soon prompted an interest in investigating the properties of a single

* Corresponding author.
E-mail address: dassarma@umd.edu (S. Das Sarma).

0038-1098/$ – see front matter © 2009 Elsevier Ltd. All rights reserved.
doi:10.1016/j.ssc.2009.02.041

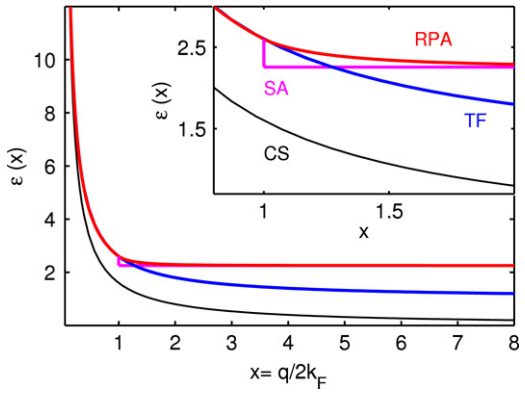

Fig. 1. The main panel shows different dielectric functions used in the literature, including the "Complete Screening" (CS), "Thomas–Fermi" (TF) and "Random Phase Approximation" (RPA). The inset is a blow-up at $q = 2k_F$ to show where the "Step Approximation" (SA) used in Ref. [27] differs from the exact result.

charged impurity embedded in graphene. Katsnelson [28] studied this problem using a Fermi–Thomas approximation, followed by studies in Refs. [29–35] which were mostly interested in effects beyond the RPA such as determining the critical impurity charge for which the Coulomb impurity forms bound states and the screening properties of graphene in the supercritical regime.

It was understood by Refs. [22,36] that as one approached the Dirac point, one would soon encounter a situation where the gate voltage induced carrier density would be smaller than the fluctuation of carrier density induced by the charged impurities thereby breaking the graphene landscape into puddles of electrons and holes. Solving numerically for the conductivity using a finite-sized Kubo formalism for a limited range of impurity concentrations, Ref. [36] concluded that the Coulomb disorder model gave a *universal* minimum conductivity whose value did not depend on the charged impurity concentration, but that was larger than that expected for clean Dirac Fermions [28,37–40], while Ref. [22] argued that this would give rise to a *non-universal* minimum conductivity whose value depended on the concentration of charged impurities. Ref. [27] developed a mean-field approach to understand the properties of graphene at the Dirac point by calculating an effective carrier density self-consistently. This theory made quantitative predictions about the dependence of the minimum conductivity and rms carrier density on the charged impurity concentration and substrate dielectric constant, and in particular argued that cleaner graphene samples would have larger minimum conductivity. Ref. [41] then studied the ground state properties of graphene by minimizing an energy functional comprising kinetic energy, Hartree, exchange [25,42,43] and correlation [25,43,44] contributions in the presence of Coulomb disorder. This work made quantitative predictions about properties of the carrier density distribution, both at and away from the Dirac point, and enabled Ref. [45] to develop an effective medium theory to calculate the graphene's conductivity through these inhomogeneous puddles, capturing quantitatively the minimum conductivity plateau that is seen in experiments [1,19,46]. We mention that underlying the existence of this minimum conductivity plateau is the high transmission of graphene p–n junctions, which has been the subject of theoretical [47,48] and experimental [49–51] studies. For the purposes of this paper we do not discuss quantum interference effects (see Ref. [52] and references therein) or the strongly interacting regime (see Ref. [53] and references therein).

The remainder of this paper is structured as follows. In Section 2 we discuss the problem of the screening of a single Coulomb impurity in the sub-critical regime as a useful toy model to understand the many-impurity problem that we address in Section 3, where we study the case of many Coulomb impurities that are uncorrelated and distributed uniformly in order to study the ground state properties of graphene. In Section 4.1, we review the high-density Boltzmann transport theory, and discuss the Effective Medium Theory (EMT) in Section 4.2. In Sections 5–7 we briefly review the experimental situation, discuss graphene's minimum conductivity, and recent theoretical work not covered in this review. We then conclude in Section 8.

2. Screening of a single Coulomb impurity

Following Ref. [28], one can construct the Thomas–Fermi screening of a single charged impurity. The goal is to calculate the screened Coulomb potential $V_s(r) = V_0(r) + V_{\rm ind}(r)$, where the bare potential $V_0 = \hbar v_F r_s [r^2 + d^2]^{-1/2}$ and the induced potential is given by

$$V_{\rm ind}(r) = (\hbar v_F r_s) \int {\rm d}\mathbf{r}' \frac{n(r') - \bar{n}}{|\mathbf{r} - \mathbf{r}'|}, \tag{1}$$

where we can imagine tuning the back gate to ensure charge neutrality $\bar{n} = 0$. If one further assumes that the local carrier density is given by the Fermi–Thomas condition, $n[V(r)] = -V(r)^2/[\pi(\hbar v_F)^2]$, one can write down a (one-dimensional) self-consistency equation for $\tilde{V}_s = V_s/\hbar v_F r_s$:

$$\tilde{V}_s(r) = \frac{1}{\sqrt{r^2 + d^2}} - \frac{4r_s^2}{\pi} \int {\rm d}r' \frac{r'}{r + r'} K\left[\frac{4rr'}{(r + r')^2}\right] \tilde{V}_s^2(r'), \tag{2}$$

where $K[x]$ is the complete elliptic integral of the first kind. The screened potential induced for this single impurity using this method was discussed in Ref. [28]. This formalism can be generalized using the method developed in Ref. [41] to include the effects of exchange. The ground state carrier density can be obtained from the Thomas–Fermi–Dirac (TFD) energy functional

$$\begin{aligned} E[n] = \hbar v_F \Bigg[& \frac{2\sqrt{\pi}}{3} \int {\rm d}^2 r \, {\rm sgn}(n) |n|^{3/2} \\ & + \frac{r_s}{2} \int {\rm d}^2 r \int {\rm d}^2 r' \frac{n(\mathbf{r}) n(\mathbf{r}')}{|\mathbf{r} - \mathbf{r}'|} + \frac{E_{xc}[n]}{\hbar v_F} \\ & + r_s \int {\rm d}^2 r V_D(\mathbf{r}) n(\mathbf{r}) - \frac{\lambda}{\hbar v_F} \int {\rm d}^2 r n(\mathbf{r}) \Bigg] \end{aligned} \tag{3}$$

where the first term in Eq. (3) is the kinetic energy, the second term is the Hartree part of the Coulomb interaction, the third term is the exchange-correlation energy and the fourth term is the energy due to disorder, where V_D is the disorder potential and the last term is added to set the average carrier density, $\langle n \rangle$, through the chemical potential λ. The correlation term is much smaller than the exchange and, to very good approximation [25,43,44], is proportional to the exchange. Therefore, hereafter, we neglect the correlation contribution by assuming $\delta E_{xc}/\delta n = \Sigma(n)$, where $\Sigma(n)$ is the Hartree–Fock self-energy [25,43,42]. The energy functional equation (3) is quite general and can be tailored by properly choosing V_D and its coupling to $n(\mathbf{r})$, to consider different sources of disorder. For the single-impurity problem, the solution can also be cast as a one-dimensional integral equation:

$$\begin{aligned} \frac{V_s(r)}{\hbar v_F} &= \frac{r_s}{\sqrt{r^2 + d^2}} + 4r_s \int {\rm d}r' \frac{r'}{r + r'} K\left[\frac{4rr'}{(r + r')^2}\right] n(r') \\ &= -{\rm sgn}(n)\sqrt{\pi |n(r)|} \left[1 + \frac{1}{4} \ln\left(\frac{4\Lambda}{\sqrt{\pi |n(r)|}}\right) \right. \\ &\quad \left. + r_s \left(\frac{2C + 1}{2\pi} + \frac{1}{8}\right)\right], \end{aligned} \tag{4}$$

where $\Lambda = 1/(0.25\ {\rm nm})$ is the band energy cutoff and $C \approx 0.916$.

3. Ground state properties at the Dirac point

The single-impurity problem discussed in the previous section is a much simpler problem because rotational symmetry makes the problem one dimensional. Adding many impurities also brings further complications: while the carrier density induced by a single impurity is negligible, this is not the case for many impurities, where although the average density can be tuned to zero via an external gate potential, the scale of the density fluctuations is set by the impurity concentration [22]. As shown in Fig. 1, the RPA screening properties of graphene are very different at the Dirac point (i.e. $k_F \to 0$) and at finite density; therefore, theoretical frameworks constructed to work at the Dirac point are bound to fail when there are such large density fluctuations. In this section, we present two different approaches to describe the Dirac point. The first is a mean-field theory where an effective density n^* is obtained by solving self-consistently for the density induced by the fluctuations of the screened impurity potential (that itself depends on the density). The second is a generalization of the energy functional method discussed above for a single impurity to the much more complicated case of many Coulomb impurities.

3.1. Self-consistent approximation (SCA)

For any microscopic single-impurity potential $\phi(r, n)$, the probability distribution, $P(V)$, of the total potential, V, is $P(V) = \langle \delta(V - \sum_{i=1}^{N_{\rm imp}} \phi(r_i, n)) \rangle_{r_i}$, where $\langle \cdots \rangle_{r_i}$ is the average over all possible disorder configurations. Assuming that the impurities' positions are uncorrelated, one can compute expressions for all moments of the induced disorder potential [54,55]. For example, the connected moment $\langle V^k \rangle_c = n_{\rm imp} \int d^2 r [\phi(r, n)]^k$. The self-consistent approximation involves obtaining the effective carrier density n^* by equating the second moment of the disorder potential with the square of the corresponding Fermi energy $\langle V^2 \rangle_c = (E_F[n^*])^2 = \pi(\hbar v_F)^2 n^*$. This self-consistent approximation then allows us to compute any correlation function at the Dirac point, although closed form analytic results are often elusive. To make analytical progress, one can map

$$\langle V(r)V(0) \rangle = n_{\rm imp} \int d\mathbf{q} [\phi(q, n^*)]^2 e^{i\mathbf{q}\cdot\mathbf{r}} \tag{5a}$$

$$\approx \frac{n_{\rm imp}(\hbar v_F)^2 K_0[r_s, d\sqrt{n^*}]}{2\pi(\xi[r_s, d\sqrt{n^*}])^2} \exp\left[\frac{-n_{\rm imp} r^2}{2(\xi[r_s, d\sqrt{n^*}])^2}\right], \tag{5b}$$

where analytic expressions for K_0 and ξ were reported in Ref. [56]. A numerical evaluation of Eq. (5a) and the Gaussian approximation Eq. (5b) is shown in Fig. 2. Within the Gaussian approximation one finds that $n_{\rm rms} = \sqrt{\langle V^4 \rangle}/[\pi(\hbar v_F)^2] \approx n^* \sqrt{3 + [n_{\rm imp} \pi \xi^2]^{-1}} \approx \sqrt{3} n^*$, where in the last equation we further assume that $n_{\rm imp} \pi \xi^2 \sim r_s^{-4} \gg 1$. This result for $n_{\rm rms}$ is particularly useful when comparing the self-consistent approximation with other methods.

3.2. Energy Functional Minimization (EFM)

To study graphene's transport properties for a distribution of charged impurities, we use Eq. (3), taking V_D to be the potential generated by a random 2D distribution $C(\mathbf{r})$ of impurity charges placed at a distance d from the graphene layer of size $L \times L$. We assume $C(\mathbf{r})$ to be on average zero and uncorrelated, and perform our calculations on a 200 nm × 200 nm square sample with a 1 nm spatial discretization. Close to the Dirac point, for a single-disorder realization, we find that the carrier density breaks up into electron–hole puddles. Since we are interested in disorder averaged quantities, we examine several disorder realizations (500–1000) and denote disordered averaged quantities by angled brackets. To characterize the density profile, we calculate the disorder averaged density–density correlation function $\langle \delta n(\mathbf{r}) \delta n(0) \rangle$, from which we can extract the root mean square $n_{\rm rms} = \sqrt{\langle \delta n(0) \delta n(0) \rangle}$, and the typical correlation length, ξ, defined in this section as the full width at half maximum (FWHM) of $\langle \delta n(\mathbf{r}) \delta n(0) \rangle$. We find [41], for typical graphene samples, that $n_{\rm rms} \approx \langle n \rangle$ for dopings as high as 10^{12} cm^{-2} and that close to the Dirac point, for $n_{\rm imp} \lesssim 10^{10}$ cm^{-2}, $n_{\rm rms}$ including exchange is three times smaller than without. We find the correlation length ξ to be of the order of 10 nm; see Fig. 3. This value suggests that the electron–hole puddles are quite small. However, a closer inspection reveals that, close to the Dirac point, the density profile is characterized by two distinct types of inhomogeneities [45]: wide regions (i.e. big puddles spanning the system size) of low density containing a number of electrons (holes) of order $n_{\rm rms} L^2$; and few narrow regions, whose size is correctly estimated by ξ, of high density containing a number of carriers of order 2. This picture is confirmed by the results shown in Fig. 4, in which the disorder averaged area fraction, A_0, over which $|n(\mathbf{r}) - \langle n \rangle| < n_{\rm rms}/10$ is plotted as a function of $n_{\rm imp}$. We see that A_0 is of order 1/3, and we also find that the area fraction over which $|n(\mathbf{r}) - \langle n \rangle|$ is less than 1/5 of $n_{\rm rms}$ is close to 50% for $n_{\rm imp} \lesssim 10^{11}$ cm^{-2}. The combination of the relatively high density in the peaks/dips and the fact that in the low-density regions $n(\mathbf{r})$ varies over scales much bigger than 10 nm guarantees that the inequality $\sqrt{\pi n}[|\nabla n|/n]^{-1} \gg 1$ is satisfied over the majority of the graphene sample and therefore justifies the use of the EFM theory. EFM should be a reasonable quantitative theory for existing graphene samples at all values of the carrier density.

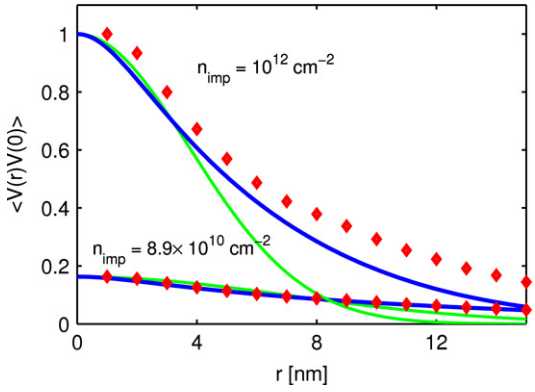

Fig. 2. Spatial correlation function for the screened potential at the Dirac point for $r_s = 0.8$ and $d = 1$ nm. Red diamonds are the results obtained by minimizing graphene's energy functional (Section 3.2). The lines are the SCA results using Eq. (5a), blue lines, and its Gaussian approximation, Eq. (5b). All the results are normalized via the value of $\langle V(0)V(0) \rangle$ for $n_{imp} = 10^{12}$ cm^{-2}.

3.3. Comparison of SCA and EFM

Here we compare the results from the Self-Consistent Approximation (SCA) of Section 3.1 and the Energy Functional Minimization (EFM) formalism discussed in Section 3.2. Fig. 2 shows the disordered averaged spatial correlation function at the Dirac point for the screened disorder potential $V = V_D + (1/2) \int d^2 r' n(\mathbf{r}')/|\mathbf{r} - \mathbf{r}'|$, where the (red) diamonds are obtained by minimizing Eq. (3). The solid (blue) line shows the same quantity calculated using the self-consistent approximation (SCA). The EFM approach and the SCA give a similar behavior for $\langle V(r)V(0) \rangle$, characterized by an algebraic, $\propto 1/r^3$, decay at large distances. The green solid line shows a Gaussian approximation which captures much of the quantitative details of the screened disorder potential correlation function, but not the power-law $1/r^3$ decay.

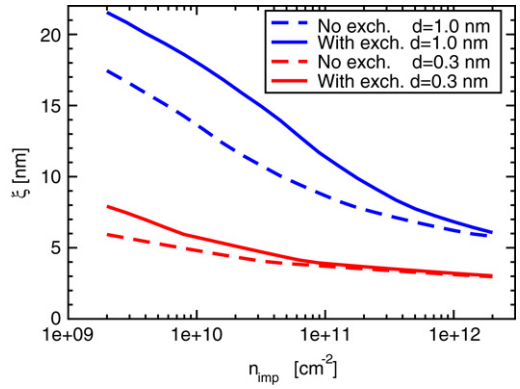

Fig. 3. Density correlation length ξ at the Dirac point as function of $n_{\rm imp}$ for $r_s = 0.8$ and two different values of d. Results with (without) exchange are shown by solid (dashed) lines.

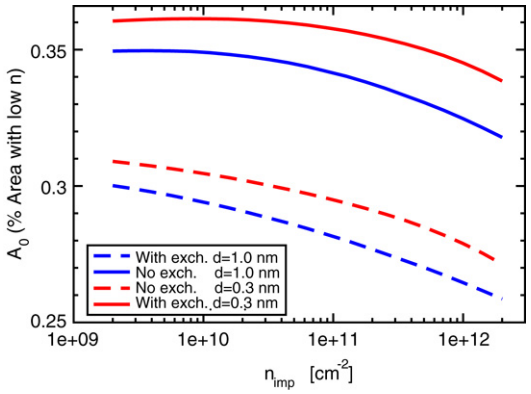

Fig. 4. Area fraction, A_0, over which is $|n(\mathbf{r}) - \langle n\rangle| < n_{\rm rms}/10$ as a function of $n_{\rm imp}$ at the Dirac point for $r_s = 0.8$. Results with (without) exchange are shown by solid (dashed) lines.

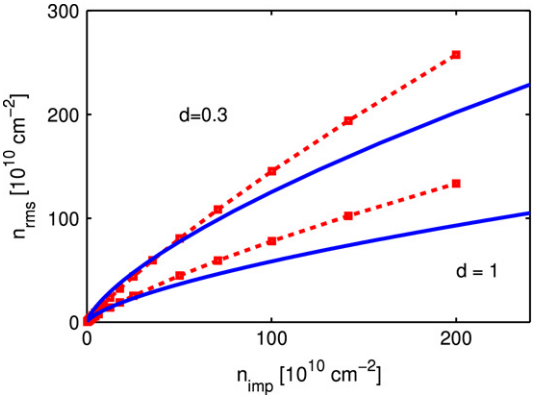

Fig. 5. Results for $n_{\rm rms}$ as a function of $n_{\rm imp}$ at the Dirac point for $r_s = 0.8$. The red dashed lines are the results obtained minimizing graphene's energy functional and the solid lines are the SCA results.

In Figs. 5–7, $n_{\rm rms}$ at the Dirac point is shown as function of $n_{\rm imp}$, r_s and d, respectively. The red dashed lines show the results obtained using the EFM theory including exchange, and the solid blue lines are the results obtained using the SCA theory. In general the SCA gives values of $n_{\rm rms}$ smaller than the EFM theory but in general there is good semi-quantitative agreement, especially at low r_s and $n_{\rm imp}$.

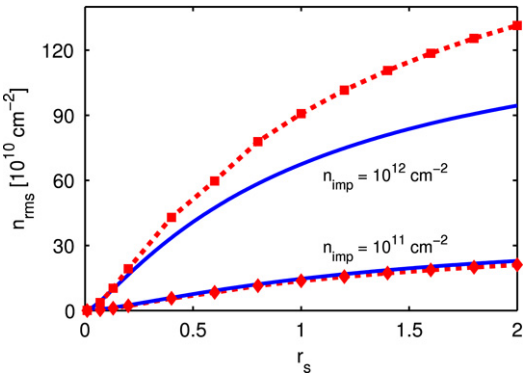

Fig. 6. Results for $n_{\rm rms}$ as a function of r_s at the Dirac point for two values of $n_{\rm imp}$ and $d = 1$ nm. The red dashed lines are the results obtained minimizing graphene's energy functional and the solid lines are the SCA results.

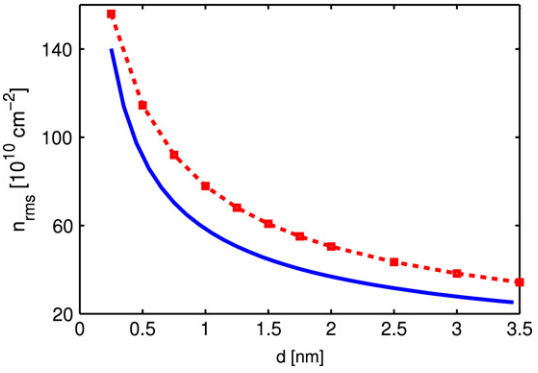

Fig. 7. Results for $n_{\rm rms}$ as a function of d at the Dirac point for $n_{\rm imp} = 10^{12}$ cm^{-2} and $r_s = 0.8$. The red dashed lines are the results obtained minimizing graphene's energy functional and the solid lines are the SCA results.

4. Graphene conductivity

4.1. High density: Boltzmann transport theory

In this section we investigate the graphene transport for large carrier densities ($n \gg n_i$), where the system is homogeneous. We show in detail the microscopic transport properties at high carrier density using the Boltzmann transport theory [57]. We calculate the conductivity σ (or mobility $\mu = \sigma/ne$) in the presence of randomly distributed Coulomb impurity charges near the surface with the electron–impurity interaction being screened by the 2D electron gas in the random phase approximation (RPA). Even though the screened Coulomb scattering is the most important scattering mechanism in our calculation, there are additional scattering mechanisms (i.e. neutral point defects) unrelated to the charged impurity scattering for very high mobility samples. Point defects gives rise to a constant conductivity in contrast to charged impurity scattering which produces a conductivity linear in n/n_i. Our formalism can include both effects, where zero range scatterers are treated with an effective point defect density of n_p. For the purpose of this calculation, we neglect all phonon scattering effects, which were considered recently with the finding that acoustic phonon scattering gives rise to a resistivity that is linear in temperature [58].

We start by assuming graphene to be a homogeneous 2D carrier system of electrons (or holes) with a carrier density n induced by the external gate voltage. The low-energy band Hamiltonian for homogeneous graphene is well approximated by a 2D Dirac equation for massless particles,

$$H = \hbar v_F(\sigma_x k_x + \sigma_y k_y), \tag{6}$$

where v_F is the 2D Fermi velocity, σ_x and σ_y are Pauli spinors and $\mathbf{k}$ is the momentum relative to the Dirac points. The corresponding eigenstates are given by the plane wave $\psi_{s\mathbf{k}}(\mathbf{r}) = \frac{1}{\sqrt{A}}\exp(i\mathbf{k}\cdot\mathbf{r})F_{s\mathbf{k}}$, where A is the area of the system, $s = \pm 1$ indicate the conduction $(+1)$ and valence (-1) bands, respectively, and $F^{\dagger}_{s\mathbf{k}} = \frac{1}{\sqrt{2}}(e^{i\theta_{\mathbf{k}}}, s)$ with $\theta_{\mathbf{k}} = \tan(k_y/k_x)$ being the polar angle of the momentum $\hbar\mathbf{k}$. The corresponding energy of graphene for the 2D wave vector $\mathbf{k}$ is given by $\epsilon_{s\mathbf{k}} = s\hbar v_F|\mathbf{k}|$, and the density of states (DOS) is given by $D(\epsilon) = g|\epsilon|/(2\pi\hbar^2 v_F^2)$, where $g = g_s g_v$ is the total degeneracy ($g_s = 2, g_v = 2$ being the spin and valley degeneracies, respectively).

When the external force is weak and the displacement of the distribution function from the thermal equilibrium value is small, we can use a linearized Boltzmann equation within the relaxation time approximation. In this case the conductivity for graphene can be written as

$$\sigma = \frac{e^2 v_F^2}{2}\int \mathrm{d}\epsilon_k D(\epsilon_k)\tau(\epsilon_k)\left(-\frac{\partial f(\epsilon_k)}{\partial \epsilon_k}\right). \tag{7}$$

Note that $f(\epsilon_k)$ is the Fermi distribution function, $f(\epsilon_k) = \{1+\exp[(\epsilon_k-\lambda)]/k_BT\}^{-1}$, where the finite temperature chemical potential $\lambda(T)$ is determined self-consistently to conserve the total number of electrons. At $T = 0, f(\epsilon)$ is a step function at the Fermi energy $E_F \equiv \lambda\,(T=0)$, and we then recover the Einstein relation $\sigma = \frac{e^2 v_F^2}{2}D(E_F)\tau(E_F)$. In Eq. (7), $\tau(\epsilon_{s\mathbf{k}})$ is the relaxation time or the transport scattering time of the collision, and it is given by

$$\frac{1}{\tau(\epsilon_{s\mathbf{k}})} = \frac{2\pi}{\hbar}\sum_a n_i^{(a)}\int \frac{\mathrm{d}^2k'}{(2\pi)^2}|\langle V^{(a)}_{s\mathbf{k},s\mathbf{k}'}\rangle|^2 \times [1-\cos\theta_{\mathbf{k}\mathbf{k}'}]\delta(\epsilon_{s\mathbf{k}}-\epsilon_{s\mathbf{k}'}), \tag{8}$$

where $\theta_{\mathbf{k}\mathbf{k}'}$ is the scattering angle between the scattering in- and out-wave vectors $\mathbf{k}$ and $\mathbf{k}'$, $\langle V^{(a)}_{s\mathbf{k},s'\mathbf{k}'}\rangle$ is the matrix element of the scattering potential associated with impurity disorder in the graphene environment, and $n_i^{(a)}$ is the number of impurities per unit area of the ath kind of impurity. Note that, since we consider elastic impurity scattering, interband processes ($s \neq s'$) are not permitted.

The matrix element of the scattering potential of randomly distributed screened impurity charge centers in graphene is given by

$$|\langle V^{(a)}_{s\mathbf{k},s\mathbf{k}'}\rangle|^2 = \left|\frac{V_i(q,d)}{\varepsilon(q)}\right|^2\frac{1+\cos\theta}{2} \tag{9}$$

where $q = |\mathbf{k}-\mathbf{k}'|, \theta \equiv \theta_{\mathbf{k}\mathbf{k}'}$, and $V_i(q,d) = 2\pi e^2\exp(-qd)/(\kappa q)$ is the Fourier transform of the 2D Coulomb potential in an effective background lattice dielectric constant κ, where d is the location of the charged impurity measured from the graphene sheet. The factor $(1+\cos\theta)/2$ arises from the sublattice symmetry (overlap of wave function) [17].

In Eq. (9), $\varepsilon(q) \equiv \varepsilon(q,T)$ is the 2D finite temperature static RPA dielectric (screening) function appropriate for graphene, given by $\varepsilon(q,T) = 1 + v_c(q)[1-G(q)]\Pi(q,T)$, where $\Pi(q,T)$ is the graphene irreducible finite-temperature polarizability function [58], $v_c(q)$ is the Coulomb interaction, and $G(q)$ is the local field correction. In the RPA, $G(q) = 0$ and in the Hubbard approximation (HA), $G(q) = 1/(g_s g_v)\times(q/\sqrt{q^2+k_F^2})$ [59].

In Fig. 8 we show the calculated graphene conductivities limited by screened charged impurities. The RPA screening used in our calculation is the main approximation. We also show results for the HA screening [59], which includes local field corrections approximately. We note that since the graphene is a weakly interacting system ($r_s < 1$) the correlation effects are not strong.

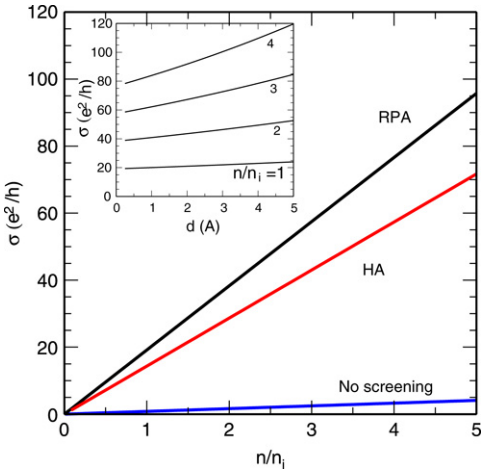

Fig. 8. Calculated graphene conductivity as a function of carrier density (n/n_i, where n_i is the impurity density) limited by Coulomb scattering. RPA (HA) indicates the result with the RPA (HA) screened Coulomb scattering, and "no screening" indicates the results with bare Coulomb scattering. Note that the calculated conductivity with unscreened Coulomb potential is less than $4e^2/h$ for the given density range. In the inset the effect of remote scatters is shown. Here d is the distance between the 2D graphene layer and the 2D impurity layer.

We emphasize that in order to get quantitative agreement with experiments, the screening effects must be included. Using the unscreened dielectric function would result in conductivity less than $4e^2/h$ for the entire range of gate voltages used in the experiment. Our main result with screened Coulomb impurities is the quantitative agreement with experiments in the regime where the conductivity is linear in density. In the inset we show the effect of remote scatterers which are located at a distance d from the interface. The main effect of remote impurity scatterings is that the conductivity deviates from the linear behavior with density and increases with both the distance d and n/n_i.

For very high mobility samples, one finds a sub-linear conductivity instead of the linear behavior with density. Such high-quality samples presumably have a small charge impurity concentration n_i, and it is therefore likely that point defects here play a more dominant role. Point defects gives rise to a constant conductivity in contrast to charged impurity scattering which produces a conductivity that is linear in n/n_i. In the presence of both the long-ranged charged impurity and the short-ranged neutral impurity, the total scattering time becomes $1/\tau_t = 1/\tau_i + 1/\tau_0$, where τ_i (τ_0) is the scattering time due to charged Coulomb (short-ranged) impurities. Shown in Fig. 9 is the graphene conductivity calculated including both charge impurity and zero range point defect scattering for different ratios of the point scatterer impurity density n_p and the charge impurity density n_i. For small n_p/n_i we find the linear conductivity that is seen in most experiments, and for large n_p/n_i we see the flattening out of the conductivity curve (which in the literature [3] has been referred to as the sub-linear conductivity). We believe this high-density flattening of the graphene conductivity is a non-universal crossover behavior arising from the competition between two kinds of scatterers. In general this crossover occurs when two scattering potentials are equivalent, that is, $n_i V_i^2 \approx n_p V_0^2$.

In the inset of Fig. 9 we show our calculated mobility in the presence of both charged impurities and short-ranged impurities. As the scattering limited by the short-ranged impurity dominates over that by the long-ranged impurity (e.g. $n_p V_0^2 \gg n_i V_i^2$) the mobility is no longer dependent on the charged impurity and approaches its limiting value,

$$\mu = \frac{e}{4\hbar}\frac{(\hbar v_F)^2}{n}\frac{1}{n_p V_0^2}. \tag{10}$$

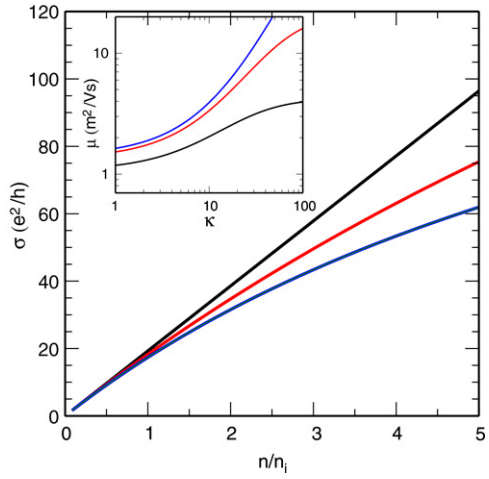

Fig. 9. Graphene conductivity calculated using a combination of short- and long-range scatterers. In this calculation, we use $n_p/n_i = 0, 0.01, 0.02$ (top to bottom). In the inset we show the graphene mobility as a function of dielectric constant (κ) of the substrate for different carrier densities $n = 0.1, 1, 5 \times 10^{12}$ cm^{-2} (from top to bottom) in the presence of both long-ranged charged impurity ($n_i = 2\times 10^{11}$ cm^{-2}) and short-ranged neutral impurity ($n_p = 0.4 \times 10^{10}$ cm^{-2}). $V_0 = 1$ keV Å^2 is used in this calculation, which corresponds to the Coulomb potential of electron density $n = 10^{12}$ cm^{-2}.

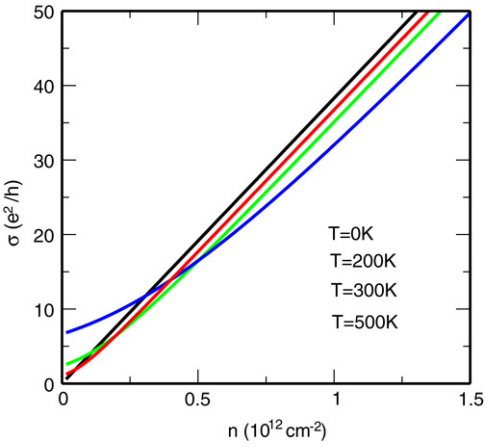

Fig. 10. Calculated conductivity for different temperatures $T = 0, 200, 300, 500$ K (top to bottom) as a function of density with an impurity density $n_i = 5\times 10^{11}$ cm^{-2}.

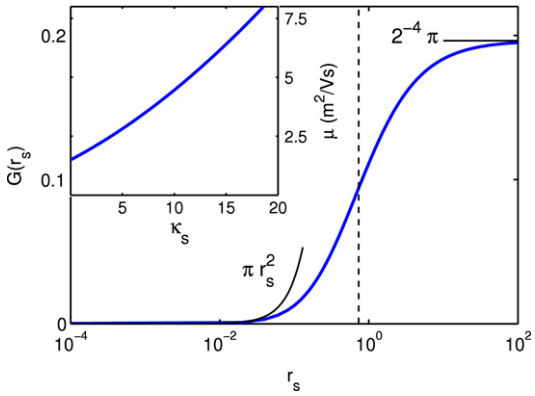

Fig. 11. The main panel shows $G[r_s]$ that parameterizes the inverse scattering time in the Boltzmann theory. The analytic form of $G[r_s]$ can be found in Ref. [27]. The dashed line shows the experimentally relevant regime for graphene on SiO_2 substrates. The inset shows the sample mobility as a function of substrate dielectric constant κ_s for $n_{\rm imp} = 2 \times 10^{11}$ cm^{-2}. Changing κ_s by a factor of 2 increases the mobility by 50%.

The limiting mobility depends only on the neutral impurity concentration n_p and carrier density.

Finally, in Fig. 10 we show the calculated temperature dependent conductivity for different temperatures as a function of density. We note that there are two independent sources of temperature dependent resistivity in our calculation. One comes from the energy averaging defined in Eq. (7), and the other is the explicit temperature dependence of the dielectric function $\varepsilon(q, T)$ which produces a temperature dependent $\tau(\varepsilon, T)$. Fig. 10 shows that in the high-density limit the conductivity decreases as the temperature increases, but in the low-density limit the conductivity shows non-monotonic behavior, i.e. $\sigma(T)$ has a local minimum at a finite temperature and increases as the temperature increases. Thus, we find that the calculated conductivity shows a non-monotonicity in the low-density limit, i.e., at low temperatures the conductivity shows metallic behavior and at high temperatures it shows insulating behavior. The non-monotonicity of the temperature dependent $\sigma(T)$ is understood to arise from temperature dependent screening [60]. We mention that for $T \gtrsim 100$ K, phonons contribute to the temperature dependence of graphene conductivity [58,61].

4.2. Low density: Effective medium theory

At low density the fluctuations in carrier density become larger than the average density. To understand the transport properties of this inhomogeneous system, Ref. [45] developed an effective medium theory where graphene's conductivity is found by solving an integral equation:

$$\int {\rm d}n \frac{\sigma[n] - \sigma_{\rm EMT}}{\sigma[n] + \sigma_{\rm EMT}} P[n] = 0 \qquad (11)$$

where $P[n]$ is the density distribution function and $\sigma[n]$ is the (local) Boltzmann conductivity discussed in Section 4.1. For the purpose of this section, we take $\sigma_B[n] = (2e^2/G[r_s]h)n/n_{\rm imp}$, where $G[r_s]$ was derived in Ref. [27] and is shown in Fig. 11. The quantitatively accurate theory using $P[n]$ derived from the EFM of Section 3.2 was developed in Ref. [45]. Here we derive analytical results obtained by using model distribution functions for $P[n]$, which as discussed in Ref. [45] show quantitative agreement with the numerical theory only for small r_s and low $n_{\rm imp}$. To illustrate this method, we first consider $P[n]$ to be a Gaussian distribution. Requiring that $\int n^2 P[n] = n_{\rm rms}^2$ fixes all the free parameters. Solving Eq. (11) then gives $z \exp^{-z^2}(\pi {\rm Erfi}[z] - {\rm Ei}[z^2]) = \sqrt{\pi}/2$, where Erfi is the imaginary error function, Ei is the exponential integral function and $z = \sigma_{\rm EMT}/(\sqrt{2}\sigma_B[n_{\rm rms}]) \approx 0.405$, giving $\sigma_{\rm EMT} \approx 0.9925\ \sigma_{\rm SCA}$, where we use the results of Section 3.1 that $\sigma_{\rm SCA} = \sigma_B[n^*]$ and $n_{\rm rms} \approx \sqrt{3}n^*$. The development of an effective medium theory for graphene [45] now allows us to reinterpret the results of Ref. [27] as equivalent to the assumption that $P[n]$ is Gaussian with density fluctuations determined by the self-consistency condition $E_{\rm F}^2 = \langle V_D^2 \rangle$.

We can explore other functional forms for $P[n]$. For a Lorentzian $P[n] = (n_L/\pi)/(n_L^2 + n^2)$, one can solve Eq. (11) analytically, giving $\sigma_{\rm EMT} = \sigma_B[n_L]$. If one identifies the width of the Lorentzian with the self-consistent carrier density $n_L = n^*$, then this provides another way to understand the self-consistent transport result. Subsequent to the results of Ref. [45], Fogler developed an effective medium theory using $P[n] = (1/\sqrt{2}\ n_{\rm rms}) \exp[-\sqrt{2}|n|/n_{\rm rms}]$, where, similar to the Gaussian distribution case, requiring normalization and setting $\langle n^2 \rangle = n_{\rm rms}^2$ fixes all the free parameters. Solving Eq. (11) gives $ze^z\Gamma[z] = 1/2$, where Γ is the Gamma function and $z = \sqrt{2}\sigma_{\rm EMT}/\sigma_B[n_{\rm rms}] \approx 0.610$. Again, approximating $n_{\rm rms} \approx \sqrt{3}n^*$, we find $\sigma_{\rm EMT} \approx 0.75\ \sigma_{\rm SCA}$, which is different from the numerical results obtained in Ref. [62]. While these analytical

approximations are useful in providing a qualitative understanding of graphene transport, quantitative differences remain between these and the full numerical solution [45], especially at large impurity concentrations and large r_s (see e.g. Fig. 6).

4.3. Suspended graphene

One of the direct consequences of charged impurity scattering in graphene is the prediction [22] that the elimination of charged impurities from the graphene environment, for example, by suspending graphene, without any substrate would lead to a much enhanced carrier mobility. Recently, Bolotin et al. [63,64] managed to remove charged impurities from the graphene environment by suspending graphene without any substrate (and simply current-annealing away any remnant impurities on the graphene surface). This immediately led to an order of magnitude increase (to $\mu \sim 10^5$ cm^2/V s) in the graphene mobility as predicted theoretically. Recent theoretical work [65] shows excellent agreement with the transport measurements on suspended graphene [63,64,66], with both the reduced impurity density and the modified screening (due to the elimination of the substrate) contributing to the graphene conductivity. Since phonon scattering effects in graphene are weak up to room temperature [58], the enhanced graphene mobility arising from the elimination of charged impurities may lead to very high ($>10^5$ cm^2/V s) graphene mobilities even at room temperature.

5. Discussion of experiments

One of the very first puzzles in graphene transport experiments [1] was that the conductivity was linear in carrier density, whereas existing theory [39] predicted constant conductivity at high density. As discussed in Section 1, the linear in density relationship emerges naturally from the Boltzmann transport theory of charged impurities [17,20–22,27], and to our knowledge, no other theory produces this linear behavior without a fine-tuning of parameters to make the scattering mimic Coulomb impurities. Moreover, three recent experiments have rigorously verified the high-density predictions of the Boltzmann transport theory. In Ref. [19], the sample mobility was correlated with the shift of the Dirac point and plateau width showing qualitative and semi-quantitative agreement with the theory presented here. Ref. [46] were able to directly measure the effect of Coulomb scatterers by intentionally adding potassium ions to graphene in ultra-high vacuum, observing qualitatively all the predictions of the (self-consistent) Boltzmann theory. Finally, Ref. [10] was able to tune graphene's fine structure constant by depositing ice on top of graphene, and thereby precisely testing predictions of the Boltzmann theory. Results from this experiment are shown in Fig. 12. Since the dielectric constant of the SiO_2 substrate and that of ice are known, there are no adjustable parameters in the theoretical curve.

6. The minimum conductivity puzzle

As described above in Section 4.2, our recent theoretical work [27,45] provides a satisfactory explanation for the minimum conductivity phenomenon in graphene near the charge neutrality (i.e. Dirac) point. In particular, early theoretical work [28,37–40] predicted a universal $T = 0$ minimum conductivity $\sigma_{\min} = 4e^2/\pi h$ at the graphene Dirac point in clean disorder-free systems. The inclusion of a disorder induced quantum anti-localization effect, assuming no intervalley scattering, leads to a theoretical infinite minimum conductivity at the Dirac point, whereas the presence of inter-valley scattering localizes the system leading to zero conductivity at the Dirac point. This confusing theoretical picture

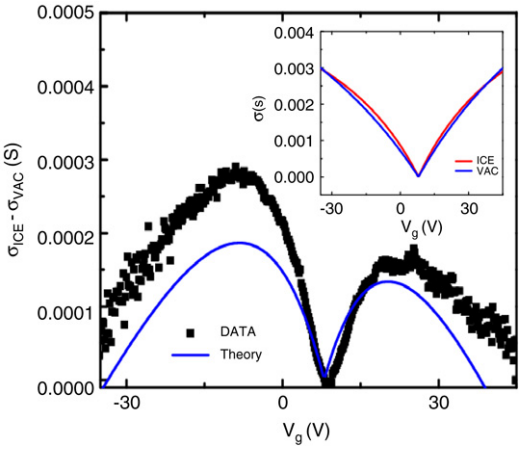

Fig. 12. Data taken from Ref. [10] show the effect of dielectric screening on graphene. The data points show the difference in graphene conductivity before and after depositing ice, while the solid line shows the theory with no adjustable parameters. The non-monotonic behavior is a consequence of the competing effects of dielectric screening on Coulomb and short-range scatterers, whereas the quantitative agreement is a stringent test of the Boltzmann theory. The inset, also taken from Ref. [10], shows the raw experimental data.

stands in stark contrast to the experimental reality, where the graphene conductivity is approximately a constant (as a function of gate voltage or carrier density) around the Dirac point, with this constant minimum conductivity plateau having a non-universal sample dependent value ($\sim 4e^2/h - 20e^2/h$).

It was first suggested in Ref. [22] that the minimum conductivity phenomenon is closely related to the break-up of the graphene landscape into inhomogeneous puddles of electrons and holes around the Dirac point due to the effect of the charged impurities in the environment. This physical idea was further developed into a quantitatively successful theory (see Section 4.2) in Refs. [27,45], where it was shown that a self-consistent treatment of the impurity induced electron–hole puddles coupled with the Boltzmann transport theory provides an excellent description of the non-universal behavior of the minimum conductivity around the Dirac point. In particular, the sample dependence of the minimum conductivity arises from the different impurity disorder in different samples.

Quantum effective field theories of graphene's minimum conductivity, which predict a universal minimum conductivity, are inapplicable to real graphene samples because real graphene is dominated by disorder induced inhomogeneity near the Dirac point, which is outside the scope of the quantum field theories. Although the self-consistent effective medium theory developed by us [27,45] gives reasonable agreement with the experimental observations, the key conceptual question of what happens at $T = 0$ as disorder also goes to zero still remains open. Such a scenario is of course experimentally irrelevant (since experiments are performed at finite temperatures in disordered systems), but the theoretical question of the conductivity crossover from the inhomogeneous Boltzmann regime of Refs. [27,45] to the homogeneous quantum transport regime is an interesting open question. Recent attempts to understand such crossover phenomena include several complementary theoretical avenues (see Refs. [52,53,67] and references therein).

7. Recent work

Among recent relevant work not discussed in this review we mention a detailed calculation of the temperature dependent graphene conductivity due to electron–phonon scattering [58], a detailed calculation of the temperature dependent graphene conductivity due to the temperature dependence of the screening of

charged impurity scattering [60], a calculation of graphene density of states as modified by impurity scattering [68], a consideration of percolation induced localization transition in graphene nanoribbons [56], a theory of charged impurity screening in graphene bilayers [69], and a prediction of graphene magnetoresistance induced by a parallel magnetic field through the spin-polarization dependence of screening [70].

8. Conclusion

We have developed here a theory for Coulomb impurities on graphene. As we have shown, Coulomb impurities behave qualitatively different from short-range scatterers such as point defects or missing atoms. Away from the Dirac point, the physics is well described by a semi-classical Boltzmann transport theory, while at the Dirac point density fluctuations dominate, breaking the system into puddles of electrons and holes. We have shown how these inhomogeneities can be characterized by a mean-field self-consistent theory and by numerically minimizing graphene's energy functional, and that an effective medium theory can be employed to describe the low-density transport properties giving semi-quantitative agreement with experimental results.

Acknowledgements

We thank Michael Fuhrer for valuable discussions. This work is supported by US-ONR and NSF-NRI-SWAN.

References

[1] K.S. Novoselov, A.K. Geim, S.V. Morozov, D. Jiang, Y. Zhang, S.V. Dubonos, I.V. Grigorieva, A.A. Firsov, Science 306 (2004) 666.
[2] K.S. Novoselov, A.K. Geim, S.V. Morozov, D. Jiang, Y. Zhang, M.I. Katsnelson, I.V. Grigorieva, S.V. Dubonos, A.A. Firsov, Nature 438 (2005) 197.
[3] Y. Zhang, Y.-W. Tan, H.L. Stormer, P. Kim, Nature 438 (2005) 201.
[4] M. Ishigami, J.H. Chen, W.G. Cullen, M.S. Fuhrer, E.D. Williams, Nano Lett. 7 (2007) 1643.
[5] E. Stolyarova, K.T. Rim, S. Ryu, J. Maultzsch, P. Kim, L.E. Brus, T.F. Heinz, M.S. Hybertsen, G.W. Flynn, Proc. Nat. Acad. Sci. 104 (2007) 9209.
[6] G.M. Rutter, J.N. Crain, N.P. Guisinger, T. Li, P.N. First, J.A. Stroscio, Science 317 (2007) 219.
[7] G. Li, E.Y. Andrei, Nature Phys. 3 (2007) 623.
[8] J. Martin, N. Akerman, G. Ulbricht, T. Lohmann, J.H. Smet, K. von Klitzing, A. Yacobi, Nature Phys. 4 (2008) 144.
[9] F. Schedin, A.K. Geim, S.V. Morozov, D. Jiang, E.H. Hill, P. Blake, K.S. Novoselov, Nature Mater. 6 (2007) 652.
[10] C. Jang, S. Adam, J.-H. Chen, E.D. Williams, S. Das Sarma, M.S. Fuhrer, Phys. Rev. Lett. 101 (2008) 146805.
[11] C. Berger, Z. Song, X. Li, X. Wu, N. Brown, C. Naud, D. Mayou, T. Li, J. Hass, A.N. Marchenkov, et al., Science 312 (2006) 1191.
[12] J.S. Bunch, A.M. van der Zande, S.S. Verbridge, I.W. Frank, D.M. Tanenbaum, J.M. Parpia, H.G. Craighead, P.L. McEuen, Science 315 (2007) 490.
[13] C. Lee, X. Wei, J.W. Kysar, J. Hone, Science 321 (2008) 385.
[14] I. Aleiner, K. Efetov, Phys. Rev. Lett. 97 (2006) 236801.
[15] A. Altland, Phys. Rev. Lett. 97 (2006) 236802.
[16] M.S. Foster, I.L. Aleiner, Phys. Rev. B 77 (2008) 195413.
[17] T. Ando, J. Phys. Soc. Japan 75 (2006) 074716.
[18] J. Gonzalez, F. Guinea, V.A.M. Vozmediano, Nuclear Phys. B 424 (1994) 595.
[19] Y.-W. Tan, Y. Zhang, K. Bolotin, Y. Zhao, S. Adam, E.H. Hwang, S. Das Sarma, H.L. Stormer, P. Kim, Phys. Rev. Lett. 99 (2007) 246803.
[20] K. Nomura, A.H. MacDonald, Phys. Rev. Lett. 96 (2006) 256602.
[21] V. Cheianov, V. Fal'ko, Phys. Rev. Lett. 97 (2006) 226801.
[22] E.H. Hwang, S. Adam, S. Das Sarma, Phys. Rev. Lett. 98 (2007) 186806.
[23] E.H. Hwang, S. Das Sarma, Phys. Rev. B 75 (2007) 205418.
[24] B. Wunsch, T. Stauber, F. Sols, F. Guinea, New J. Phys. 8 (2006) 318.
[25] Y. Barlas, T. Pereg-Barnea, M. Polini, R. Asgari, A.H. MacDonald, Phys. Rev. Lett. 98 (2007) 236601.
[26] M. Polini, R. Asgari, Y. Barlas, T. Pereg-Barnea, A. MacDonald, Solid State Commun. 143 (2007) 58.
[27] S. Adam, E.H. Hwang, V.M. Galitski, S. Das Sarma, Proc. Natl. Acad. Sci. USA 104 (2007) 18392.
[28] M.I. Katsnelson, Phys. Rev. B 74 (2006) 201401.
[29] A.V. Shytov, M.I. Katsnelson, L.S. Levitov, Phys. Rev. Lett. 99 (2007) 236801.
[30] V.M. Pereira, J. Nilsson, A.H. Castro Neto, Phys. Rev. Lett. 99 (2007) 166802.
[31] R.R. Biswas, S. Sachdev, D.T. Son, Phys. Rev. B 76 (2007) 205122.
[32] D.S. Novikov, Appl. Phys. Lett. 91 (2007) 102102.
[33] M.M. Fogler, D.S. Novikov, B.I. Shklovskii, Phys. Rev. B 76 (2007) 233402.
[34] I.S. Terekhov, A.I. Milstein, V.N. Kotov, O.P. Sushkov, Phys. Rev. Lett. 100 (2008) 076803.
[35] V.M. Pereira, V.N. Kotov, A.H. Castro Neto, Phys. Rev. B 78 (2008) 085101.
[36] K.A. Nomura, H. MacDonald, Phys. Rev. Lett. 98 (2007) 076602.
[37] E. Fradkin, Phys. Rev. B 33 (1986) 3257.
[38] A.W.W. Ludwig, M.P.A. Fisher, R. Shankar, G. Grinstein, Phys. Rev. B 50 (1994) 7526.
[39] N. Shon, T. Ando, J. Phys. Soc. Japan 67 (1998) 2421.
[40] J. Tworzydło, B. Trauzettel, M. Titov, A. Rycerz, C.W.J. Beenakker, Phys. Rev. Lett. 96 (2006) 246802.
[41] E. Rossi, S. Das Sarma, Phys. Rev. Lett. 101 (2008) 166803.
[42] E.H. Hwang, B.Y.-K. Hu, S. Das Sarma, Phys. Rev. Lett. 99 (2007) 226801.
[43] S. Das Sarma, E.H. Hwang, W.-K. Tse, Phys. Rev. B 75 (2007) 121406.
[44] M. Polini, A. Tomadin, R. Asgari, A.H. MacDonald, Phys. Rev. B 78 (2008) 115426.
[45] E. Rossi, S. Adam, S. Das Sarma, 2008. arXiv:0809.1425.
[46] J.H. Chen, C. Jang, S. Adam, M.S. Fuhrer, E.D. Williams, M. Ishigami, Nature Phys. 4 (2008a) 377.
[47] V. Cheianov, V.I. Fal'ko, Phys. Rev. B 74 (2006) 041403.
[48] M.M. Fogler, D.S. Novikov, L.I. Glazman, B.I. Shklovskii, Phys. Rev. B 77 (2008) 075420.
[49] B. Huard, J.A. Sulpizio, N. Stander, K. Todd, B. Yang, D. Goldhaber-Gordon, Phys. Rev. Lett. 98 (2007) 236803.
[50] J.R. Williams, L. Dicarlo, C.M. Marcus, Science 317 (2007) 638.
[51] B. Özyilmaz, P. Jarillo-Herrero, D. Efetov, D.A. Abanin, L.S. Levitov, P. Kim, Phys. Rev. Lett. 99 (2007) 166804.
[52] S. Adam, P.W. Brouwer, S. Das Sarma, 2008. arXiv:0811.0609v1.
[53] M. Mueller, L. Fritz, S. Sachdev, Phys. Rev. B 78 (2008) 115406.
[54] V. Galitski, S. Adam, S. Das Sarma, Phys. Rev. B 76 (2007) 245405.
[55] S. Adam, S. Das Sarma, Phys. Rev. B 77 (2008) 115436.
[56] S. Adam, S. Cho, M.S. Fuhrer, S. Das Sarma, Phys. Rev. Lett. 101 (2008) 046404.
[57] S. Das Sarma, E.H. Hwang, Phys. Rev. Lett. 83 (1999) 164.
[58] E.H. Hwang, S. Das Sarma, Phys. Rev. B 77 (2008) 115449.
[59] M. Jonson, J. Phys. C 9 (1976) 3059.
[60] E.H. Hwang, S. Das Sarma, 2008. arXiv:0811.1212v1.
[61] J.H. Chen, C. Jang, S. Xiao, M. Ishigami, M.S. Fuhrer, Nat. Nanotechnology 3 (2008) 206.
[62] M.M. Fogler, 2008. arXiv:0810.1755v1.
[63] K. Bolotin, K. Sikes, Z. Jiang, G. Fudenberg, J. Hone, P. Kim, H. Stormer, Solid State Commun. 146 (2008a) 351.
[64] K.I. Bolotin, K.J. Sikes, J. Hone, H.L. Stormer, P. Kim, Phys. Rev. Lett. 101 (2008b) 096802.
[65] S. Adam, S. Das Sarma, Solid State Commun. 146 (2008) 356.
[66] X. Du, I. Skachko, A. Barker, E. Andrei, Nat. Nanotechnology 3 (2008) 491.
[67] V. Cheianov, V. Fal'ko, B. Altshuler, I. Aleiner, Phys. Rev. Lett. 99 (2007) 176801.
[68] B.Y. Hu, E.H. Hwang, S. Das Sarma, Phys. Rev. B 78 (2008) 165411.
[69] E.H. Hwang, S. Das Sarma, Phys. Rev. Lett. 101 (2008) 156802.
[70] E.H. Hwang, S. Das Sarma, 2008. arXiv:0812.0403v1.